The Company of **Biologists**

RESEARCH ARTICLE

Role of a versatile peptide motif controlling Hox nuclear export and autophagy in the *Drosophila* fat body

Marilyne Duffraisse[1], Rachel Paul[1], Julie Carnesecchi[2], Bruno Hudry[3], Agnes Banreti[3], Jonathan Reboulet[1], Leiore Ajuria[1], Ingrid Lohmann[2] and Samir Merabet[1,*]

ABSTRACT

Hox proteins are major regulators of embryonic development, acting in the nucleus to regulate the expression of their numerous downstream target genes. By analyzing deletion forms of the *Drosophila* Hox protein Ultrabithorax (Ubx), we identified the presence of an unconventional nuclear export signal (NES) that overlaps with a highly conserved motif originally described as mediating the interaction with the PBC proteins, a generic and crucial class of Hox transcriptional cofactors that act in development and cancer. We show that this unconventional NES is involved in the interaction with the major exportin protein CRM1 (also known as Embargoed in flies) *in vivo* and *in vitro*. We find that this interaction is tightly regulated in the *Drosophila* fat body to control the autophagy-repressive activity of Ubx during larval development. The role of the PBC interaction motif as part of an unconventional NES was also uncovered in other *Drosophila* and human Hox proteins, highlighting the evolutionary conservation of this novel function. Together, our results reveal the extreme molecular versatility of a unique short peptide motif for controlling the context-dependent activity of Hox proteins both at transcriptional and non-transcriptional levels.

KEY WORDS: Hox protein, Ultrabithorax, Hexapeptide, Embargoed, CRM1, Nuclear export signal

INTRODUCTION

Hox proteins are key developmental regulators that act throughout embryogenesis to specify cell fates and morphogenesis along longitudinal axes in cnidarian and bilaterian animals. These homeodomain (HD)-containing transcription factors (TFs) have specific functions *in vivo*, yet recognize highly similar DNA-binding sites *in vitro* (Mann et al., 2009). It has long been postulated that Hox proteins interact with additional transcriptional partners to solve this *in vivo*/*in vitro* paradox (Mann et al., 2009). The best-characterized cofactors to date are the PBC and Meis proteins, which belong to the TALE-class of HD-containing TFs (Mukherjee and Bürglin, 2007). However, these cofactors are expressed in many tissues of the embryo and interact with the large majority of Hox proteins (Mann et al., 2009), and, therefore, cannot account for the full specificity of the Hox regulatory repertoire. In addition, molecular dissections of vertebrate and invertebrate Hox proteins have revealed the important role of the HD and its immediate

surrounding region (Merabet et al., 2009), which includes a conserved short linear interaction motif called the hexapeptide (HX) or W-containing motif because it contains an invariant tryptophan residue lying at a variable distance upstream of the HD (Morgan et al., 2000; Merabet and Mann, 2016). This tryptophan residue is important for recruiting the PBC cofactor in dimeric Hox–PBC complexes (Mann et al., 2009). Hox proteins do, however, contain a number of additional short peptide motifs that are conserved to different evolutionary extents (Merabet et al., 2009), as well as long disordered regions (Merabet and Dard, 2014). Recent work has shown that human HOX proteins can use various combinations of short peptide motifs, including the W-containing motif, to interact with the PBC and Meis cofactors, and that the long disordered regions can be engaged in non-specific interactions with various types of transcription factors (Dard et al., 2018). More generally, Hox proteins are known to contain a widespread distribution of numerous short linear interaction motifs (SLiMs), underlining that Hox functions can rely on a large and so-far poorly investigated portion of their protein sequence (Merabet and Dard, 2014; Rinaldi et al., 2018).

Here, we describe a novel role of the W-containing motif as part of an unconventional nuclear export signal (NES) in the *Drosophila* Hox protein Ultrabithorax (Ubx). We find that the activity of this unconventional NES is tightly regulated during larval development, providing a means to control the repressive function of Ubx on autophagy in the fat body. The W-containing motif was also found to be part of an unconventional NES in other *Drosophila* and human Hox proteins, highlighting that this novel function is evolutionarily conserved.

Overall our work reveals an astonishing level of functional diversity for a short conserved peptide motif, ranging from transcriptional regulation with generic or tissue-specific cofactors (Baëza et al., 2015) to context-dependent nuclear export. Thus, the W-containing motif and its immediate surrounding region constitute a privileged platform for diversifying Hox protein function at multiple levels during development and evolution.

RESULTS

N-terminal deletions lead to cytoplasmic localization of Ubx

One of the best-characterized Hox proteins in *Drosophila* is Ubx, which has been the subject of several molecular dissections to identify protein motifs and regions involved in the context of specific regulatory functions (Liu et al., 2008; Merabet et al., 2007; Lelli et al., 2011; Tour et al., 2005). Intrinsic determinants involved in the context of Hox generic regulatory functions are much less characterized, and we decided to tackle this issue for Ubx in the context of autophagy repression in the larval fat body. This function is shared by different Hox proteins in *Drosophila* (Banreti et al., 2014) and has accordingly been classified as a generic Hox function (Saurin et al., 2018). More particularly, the expression of Hox

[1]Institut de Génomique Fonctionnelle de Lyon, ENS-Lyon, 32/34 Av. Tony Garnier, 69007 Lyon, France. [2]Centre for Organismal Studies, Im Neuenheimer Feld 230, 69120 Heidelberg, Germany. [3]Institut de Biologie Valrose, Parc Valrose, 06108 Nice, France.

*Author for correspondence (samir.merabet@ens-lyon.fr)

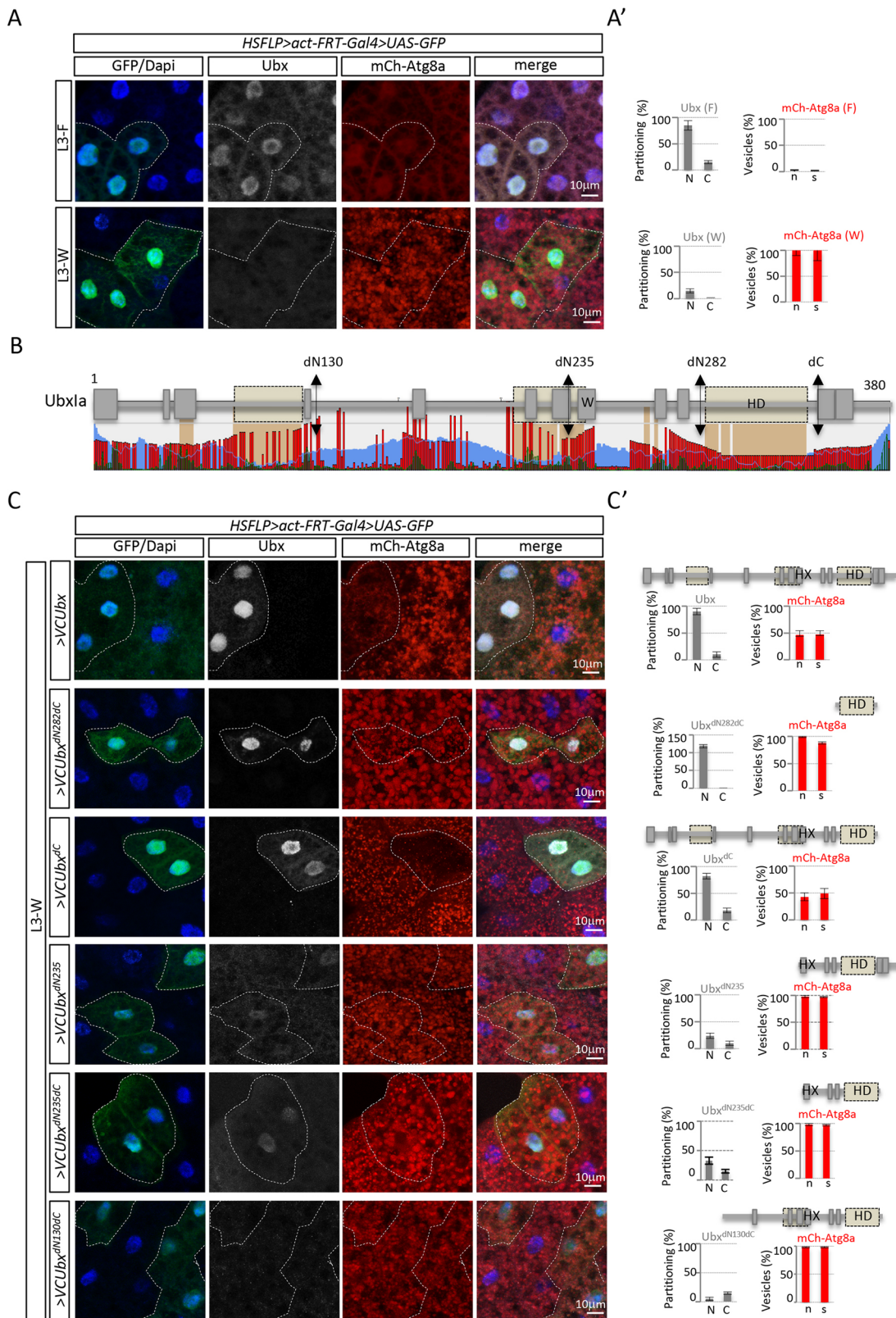L.A., 0000-0001-5375-3370; S.M., 0000-0001-7629-703X

Fig. 1. See next page for legend.

proteins in the fat body of L3-feeding (L3-F) larvae is important to repress the transcription of autophagy-related genes (*atg* genes). The loss of Hox expression in older L3-wandering (L3-W) larvae allows the transcriptional de-repression of several *atg* genes, leading to the strong induction of autophagy before metamorphosis.

We confirmed that Ubx was present in the nucleus of fat body cells until late L3-F, and that no or very low nuclear Ubx proteins could be detected at the L3-W stage (Fig. 1A,A′).

To identify part(s) of Ubx that could be important for repressing autophagy, we performed a systematic analysis based on the

Fig. 1. Effects of N-terminal deletions on the nuclear localization of Ubx in larval fat body cells. (A) Immunostaining of endogenous Ubx (gray) in the fat body of L3-feeding (L3-F) and L3-wandering (L3-W) larva. Clones (dashed lines) were induced from L1 to L3 larval stages through the leaky expression of the HSFLP promoter and are recognized with GFP expression. Nuclei are stained with DAPI (blue). The mCherry–Atg8 reporter (mCh-Atg8a; red) follows the off (weak nuclear expression) and on (dotted red staining corresponding to autophagosomes) states of autophagy in the fat body of L3-F and L3-W larvae, respectively. Scale bars: 10 μm. (A′) Graphs showing the mean±s.d. distribution (percentage of cells) with Ubx staining in the nucleus (N) or cytoplasm (C), together with the number (n) and size (s) of mCherry–Atg8 vesicles in fat body cells (also see Materials and Methods). (B) Schematic representation of Ubx1a protein isoform (corresponding to the ubiquitously expressed and major Ubx isoform in *Drosophila*) based on SLiMPred. SLiMPred applies machine learning techniques to predict new motifs based on annotated instances from the Eukaryotic Linear Motif database, as well as structural, biophysical and biochemical features derived from the protein primary sequence (Mooney et al., 2012). Prediction of short linear interaction motifs (SLiMs, green peaks), disordered regions (blue waves), ordered domains (brown boxes) and level of conservation of each residue (red peaks) is shown alongside Ubx1a. The level of conservation outside the HD, and more particularly in the N-terminal region, is due to the number of *Drosophila* species (11 species of 16 total) included in the SliMPred analysis. N- and C-terminal deletions used in this study are indicated, as well as the tryptophan (W)-containing motif and the homeodomain (HD). A simplified representation of Ubx is shown below the global structure. Boxes denote SLiMs. (C) Clones induced from L1 to L3 larval stages through the leaky expression of the HSFLP promoter are recognized by the GFP expression (green, surrounded by a white-dotted line), and Ubx constructs are revealed with an anti-Ubx (full-length Ubx constructs) or anti-HA (truncated Ubx constructs) antibody (gray). DAPI (blue) stains for nuclei and mCherry–Atg8 for autophagy (red). Scale bars: 10 μm. (C′) Graphs showing the mean±s.d. distribution of VC–Ubx constructs and mCherry–Atg8 as in A′. A schematic representation of each construct is shown above the graphs. Results represent of acquisitions from five different dissected fat bodies from at least three independent experiments. The minimal dN282dC form is localized in the nucleus but is not able to inhibit autophagy. The N-terminal deletions affect the nuclear localization and autophagy repression.

prediction of the global organization in terms of domains, disorganized regions and short linear motifs by using SLiMPred (http://bioware.ucd.ie/~compass/biowareweb/Server_pages/slimpred. php). We distinguished five different regions (Fig. 1B) that could be analyzed individually or in combination upon N- and C-terminal deletions (Fig. 1B). The resulting deleted forms were fused at their N-terminus to the C-terminal fragment of the fluorescent Venus protein (VC; Fig. S1) for subsequent protein interaction analyses (see below). Each construct was clonally expressed at the L3-W stage to test for its ability to repress autophagy in an otherwise wild-type fat body tissue, as previously described (Banreti et al., 2014). The nuclear localization of each construct was also systematically verified. As expected, the wild-type VC–Ubx construct was correctly expressed in the nucleus and led to significant repression of autophagy (Fig. 1C,C′). The minimal form of Ubx (VC–Ubx^{dN282dC}), which corresponds to the HD only, was strongly expressed in the nucleus but did not lead to autophagy repression, showing that additional region(s) to the DNA-binding domain are needed for proper autophagy repressive activity (Fig. 1C,C′). Deleting the C-terminal region downstream of the HD (construct VC–Ubx^{dC}) affected neither the nuclear localization nor the autophagy repressive activity when compared to full-length Ubx (Fig. 1C,C′). In contrast, deleting the first 235 residues (construct VC–Ubx^{dN235}) strongly affected both the nuclear localization and autophagy-repressive activity of Ubx (Fig. 1C,C′). The combined deletion of the C-terminal part (construct VC–Ubx^{dN235dC}) did not further affect the nuclear location and autophagy repression (Fig. 1C,C′). Finally, Ubx nuclear localization was even more affected upon a smaller N-terminal deletion removing the first

130 residues (construct VC–Ubx^{dN130dC}) with a consequent lack of proper autophagy-repressive activity (Fig. 1C,C′).

The fact that we could not detect N-terminally deleted Ubx forms in fat body cells suggest that these constructs were either not correctly produced, which was unlikely given that they were all inserted at the same genomic locus (see Materials and Methods), or were not correctly targeted to the nucleus and degraded. To discriminate between the two possibilities, we expressed Ubx constructs in the epidermis of the embryo, using an *Ubx-Gal4* driver to induce expression resembling endogenous Ubx levels (Duffraisse et al., 2014). The analysis showed that the VC–Ubx^{dN130dC} construct was present in the cytoplasm of half of the expressing cells, and this proportion was even higher with the Ubx^{dN235dC} construct (almost all expressing cells had cytoplasmic expression; Fig. S1). Thus, N-terminal deletions lead to a cytoplasmic localization for Ubx, a phenomenon that is normally not observed in the context of full-length Ubx in the embryo. These observations suggest the presence of an NES that is active in the context of N-terminally deleted Ubx proteins. More particularly, the respective cytoplasmic or nuclear localization of the VC–Ubx^{dN235dC} and VC–Ubx^{dN282dC} constructs (Fig. S1) indicates that the region located between the two N-terminal deletions could be instructive for the cytoplasmic localization.

Identification of an atypical NES that overlaps with the W-containing motif in Ubx

To identify putative NES(s), we scanned the Ubx protein sequence with two different algorithms, LocNES (http://prodata.swmed.edu/LocNES/LocNES.php) and NetNES (http://www.cbs.dtu.dk/services/NetNES/). Surprisingly, NetNES did not predict any NES with a significant confidence score (Fig. 2A), whereas LocNES identified three putative NES with high or low confidence scores, with two of them located in the N-terminal region (residues 37–50 and 191–205) and the other one in the HD (residues 318–332). Importantly, neither NetNEs nor LocNES predicted a putative NES in the region discriminating exported (Ubx^{dN235dC}) and non-exported (Ubx^{dN282dC}) Ubx constructs.

Although NESs are of variable nature, they all contain four or five hydrophobic residues (often isoleucine, leucine, methionine, phenylalanine and/or valine) arranged in a particular pattern (Fung et al., 2017). NESs can still adopt diverse conformations and have been classified in ten different categories (Fung et al., 2017). Interestingly, we found that the disorganized Ubx protein region comprised between the dN235 and dN282 deletions contained a sequence that could resemble to a NES but in an inverted orientation (LDSRIKGAIAM; Fig. 2A). Inverted NES sequences have been described in some instances and classified as class1a-R NESs (Fung et al., 2015, 2017). Moreover, this putative NES is conserved in flies (Fig. S1), with the last hydrophobic residue lying in the core W-containing motif (Fig. 2A).

To assess whether this sequence works as a NES in Ubx, we first tested the original HX mutation (Galant et al., 2002), which transforms the last methionine residue of the putative NES into an alanine residue (YPWM mutated into YAAA; Fig. 2A). Mutation of hydrophobic residues into alanine residues is classically used to mutate NES (Romero et al., 2008). The effect was analyzed in the context of full-length Ubx and the dN130dC deleted form, which was barely localized in the nucleus of fat body cells. Although the HX mutation did not change the nuclear localization and repressive activity of full-length Ubx, it was sufficient to induce the nuclear localization and autophagy repression with the VC–Ubx^{dN130dC} construct, at levels similar to those observed for wild-type Ubx (Fig. 2B,B′). To further confirm that this effect was due to the
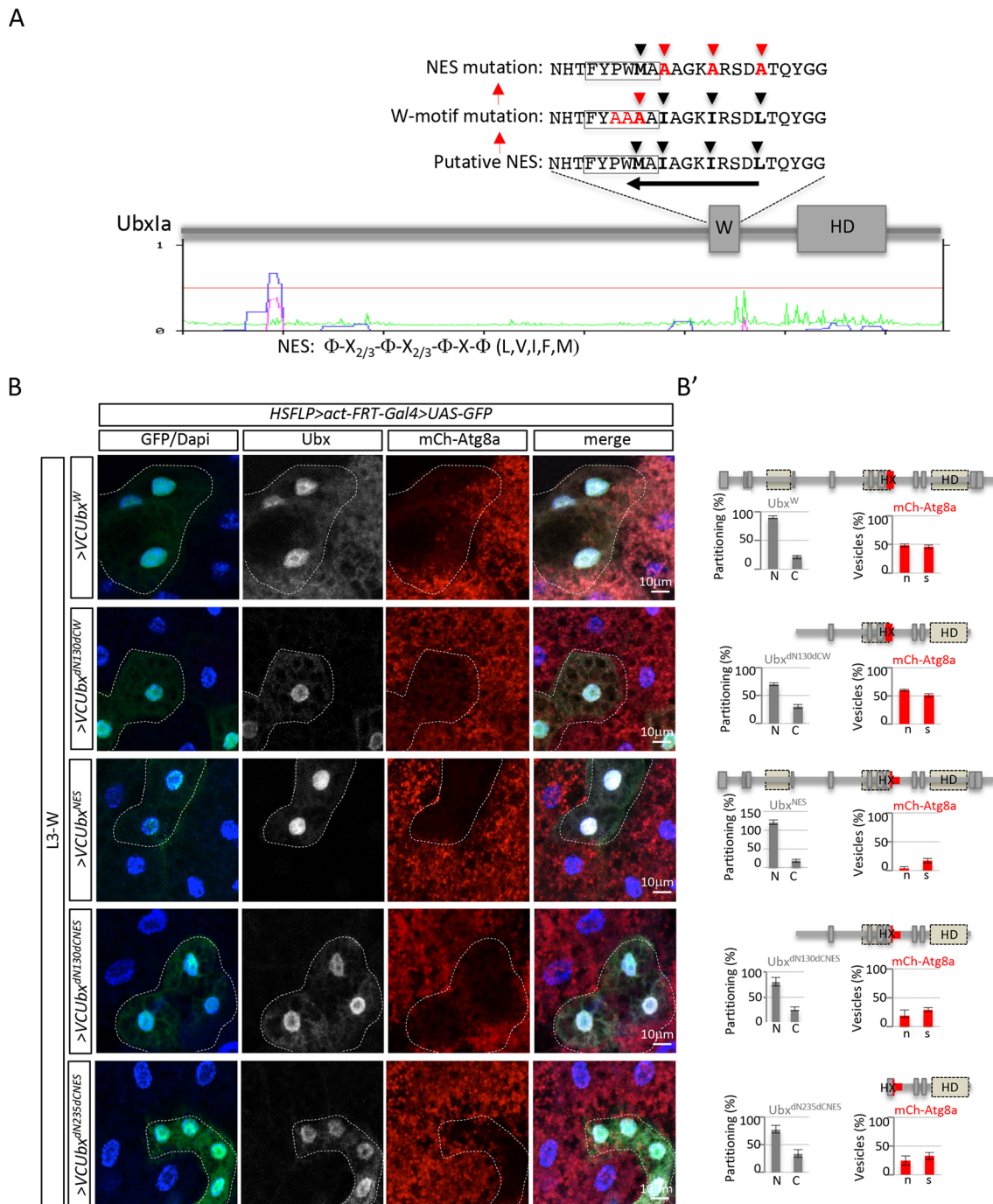
Fig. 2. Identification of an unconventional NES in the W-containing motif region of Ubx. (A) Sequence of the W-motif containing region in Ubx. The W-containing motif is boxed and hydrophobic residues that could participate in the NES are indicated (black arrowheads). The consensus NES is given below the predicted graph for full Ubx (from NetNES). Red lines in the graph indicate the threshold above which residues could be considered as part of a putative NES (from green to blue and magenta with higher significance). No full putative NES is predicted with enough statistical significance along the UbxIa protein sequence. Sequences for the mutation of the W-containing motif and NES used in this study are indicated (residues highlighted in red). Mutations affecting the putative NES do not touch the W-containing motif. The black arrow indicates the orientation of the putative NES. (B) Clones (outlined with dashed lines) expressing the NES-mutated constructs in the fat body of L3-W larva, as described in Fig. 1. Scale bars: 10 µm. (B′) Graphs showing the mean±s.d. distribution of VC–Ubx constructs and mCherry–Atg8 reporter, as described in Fig. 1. Compared to wild-type Ubx, the NES mutation induces statistically higher levels of nuclear localization and autophagy repression in the context of the full-length protein (P-value of $2.15×10^{-10}$ and $4.58×10^{-10}$, respectively; t-test). The NES mutation blocks the nuclear export induced by the N-terminal deletions, allowing the expressed proteins to reside in the nucleus and inhibit autophagy.

destabilization of the putative NES, we generated an additional set of mutations that changed the core three hydrophobic residues of the NES without disturbing the integrity of the W-containing motif (mutation named 'NES'; Fig. 2A). This additional NES mutation was analyzed in the context of full-length and deleted forms of Ubx. Results showed that the mutation of core NES residues (construct VC–Ubx^NES) induced statistically stronger levels of nuclear localization and autophagy repression than wild-type Ubx (Fig. 2B,

B′). Compared to the YAAA mutation, the mutation of core NES hydrophobic residues also led to higher nuclear localization and autophagy repression for the deletion forms of Ubx (constructs VC–Ubx^{dN130dCNES} and VC–Ubx^{dN235dCNES}; Fig. 2B,B′). The loss of cytoplasmic and gain of nuclear localizations of the N-terminally deleted forms was also observed in the epidermis of the embryo (Fig. S1). Together, these results confirmed that the W-containing motif is part of an unconventional NES that is responsible for the cytoplasmic localization of N-terminally deleted forms of Ubx.

Nuclear export is ensured in *Drosophila* by the major exportin called Embargoed (Emb, Collier et al., 2000), a homolog of vertebrate CRM1 (Adachi and Yanagida, 1989; Fornerod et al., 1997; Fukuda et al., 1997; Stade et al., 1997). To assess whether the newly identified NES motif in Ubx could be important for recruiting Emb, we performed a series of different complementary interaction assays. First, we performed bimolecular fluorescence complementation (BiFC; Kerppola, 2013) between full-length Ubx fused to the C-terminal fragment of Venus (construct VC–Ubx) and Emb fused to the complementary N-terminal fragment of Venus (construct VN–Emb). BiFC was performed with wild-type or NES-mutated Ubx. Fusion constructs were expressed with the *Ubx-Gal4* driver and BiFC was analyzed in the live embryo, as previously described (Duffraisse et al., 2014; Hudry et al., 2011). Results showed that Ubx could interact with Emb, both in the nucleus and the cytoplasm (Fig. 3A,A′). In comparison, BiFC with NES-mutated Ubx was strongly affected, as fluorescence was completely lost in the cytoplasm and decreased by 40% in the nucleus (Fig. 3A,A′).

The specific and NES-dependent activity of Emb was confirmed independently of BiFC, by co-expressing VC–Ubx with a the non-fluorescent HA-tagged Emb with the *Engrailed* (*En*)-*Gal4* driver. In this context, the forced co-expression of Emb was sufficient to induce the cytoplasmic localization of both VC–Ubx and endogenous En, which was used as an internal control for the experiment (Fig. 3B). Importantly, this cytoplasmic localization was not observed when the NES-mutated form of Ubx was co-expressed with Emb (as confirmed with cytoplasmic En; Fig. 3B), indicating that the Emb-dependent export of Ubx was fully dependent on the integrity of the newly identified NES.

Finally, the physical and NES-dependent interaction between Ubx and Emb was also assessed by GST pulldown experiments by using *in vitro* produced wild-type or NES-mutated GST–Ubx, and S2R+ cells extracts expressing HA-tagged Emb (see Materials and Methods). Control experiments showed that the NES mutation did not affect the interaction with the Exd cofactor, as expected (Fig. 3C). The direct interaction between Ubx and Emb was also confirmed and, importantly, the pulldown of Emb associated with Ubx was significantly reduced when the NES was mutated (54% loss on average, *P*=0.0084, Fig. 3C′).

The W-containing motif acts as a NES in other *Drosophila* and non-*Drosophila* Hox proteins

Given its conservation among the Hox family members, we wondered whether the W-containing motif could be part of a putative NES in other *Drosophila* Hox proteins. As previously done with Ubx, we used available scripts based on published NES sequences to scan several *Drosophila* (Deformed, Dfd; Sex combs reduced, Scr; Antennapedia, Antp; AbdominalA, AbdA; AbdominalB, AbdB) and human (HOXB4, HOXA5, HOXA7 and HOXA9) Hox proteins. This analysis did not reveal any consensus NES sequence with high confidence in the W-containing motif region, except for AbdB, which had a derived W-containing motif (corresponding to a single W residue). Surprisingly, our own analysis again revealed the presence

of a putative NES in the W-containing motif region of Dfd and Scr (Fig. S2). In contrast to Ubx, these putative NES sequences were not inverted, belonging to the class-1a, and include the W-containing motif. Moreover, the hydrophobic residues of these putative NESs are widely conserved among invertebrate and vertebrate species, suggesting they could be of functional significance.

The putative role of the NES of Dfd and Scr was assessed *in vivo* as previously done with Ubx. Since the W-containing motif was fully included in the putative NES, we used previously generated mutant Scr and Dfd proteins for the W-containing motif (Hudry et al., 2012), although these mutations affects only one core hydrophobic residue, as noticed for the W-containing motif mutation of Ubx (Fig. S2). Results showed that the mutation of the W-containing motif abolished BiFC in the cytoplasm but had no effect on the nuclear Hox–Emb interaction (Fig. S2). Co-expression of wild-type or mutated Hox proteins with non-fluorescent Emb also confirmed that the cytoplasmic localization induced by Emb was fully dependent on the W-containing motif integrity (Fig. S2). These results thus demonstrate that the W-containing motif of Dfd and Scr is required for Emb-dependent cytoplasmic localization.

The mutation of the W-containing motif in Scr also significantly affected the interaction with Emb *in vitro* (30% loss on average, *P*=0.0017; Fig. S3), although to a lesser extent than observed with the NES mutation of Ubx, which could be explained by the fact that only one core NES hydrophobic residue is affected in the context of mutated Scr.

The role of the W-containing motif as a NES was also extended to the human HOXA5 protein, as revealed by co-expressing wild-type HOXA5 or HOXA5 with a mutated W-containing motif together with CRM1 in HEK-293T cells. We observed that the cytoplasmic localization of HOXA5 induced by the co-expression of human CRM1 was fully dependent on the integrity of the W-containing motif (Fig. S3). Thus, analysis with different Hox proteins shows that the W-containing motif can be part of a functional NES in several vertebrate and invertebrate Hox proteins. The novel NES function of the W-containing motif region is therefore an evolutionary conserved molecular feature among the Hox family members.

To further validate that the W-containing motif could work as an autonomous NES, we fused the corresponding sequence of Ubx or Scr upstream of the Dronpa fluorescent protein and analyzed the nuclear and cytoplasmic localization in the embryo and larval fat body cells. Control constructs with full-length Ubx or a consensus NES sequence (Roth et al., 2003) fused to Dronpa confirmed the localization of the fluorescent reporter in the nucleus or the cytoplasm in both tissues, respectively (Fig. 3D–D″). Importantly, the fusion of Dronpa with the W-containing motif of Ubx or Scr led to its cytoplasmic localization with the same efficiency as the consensus NES sequence in both tissues (Fig. 3D–D″), validating that these peptide sequences could act as autonomous NES.

Ubx nuclear export is active and tightly regulated in the *Drosophila* larval fat body

The lack of Hox nuclear expression at the L3-W stage coincides with the onset of developmental autophagy, highlighting the importance of Hox nuclear clearance for the temporal control of autophagy. Although it has been described that Hox genes were transcriptionally repressed (Banreti et al., 2014), our results strongly suggest that Hox nuclear clearance could also rely on active nuclear export at the L3-W stage. In this scenario, nuclear export will be linked to quick degradation of the Hox protein. To assess for the functional importance of the nuclear export in the control of Hox repressive activity, we first abolished the expression of *emb* by
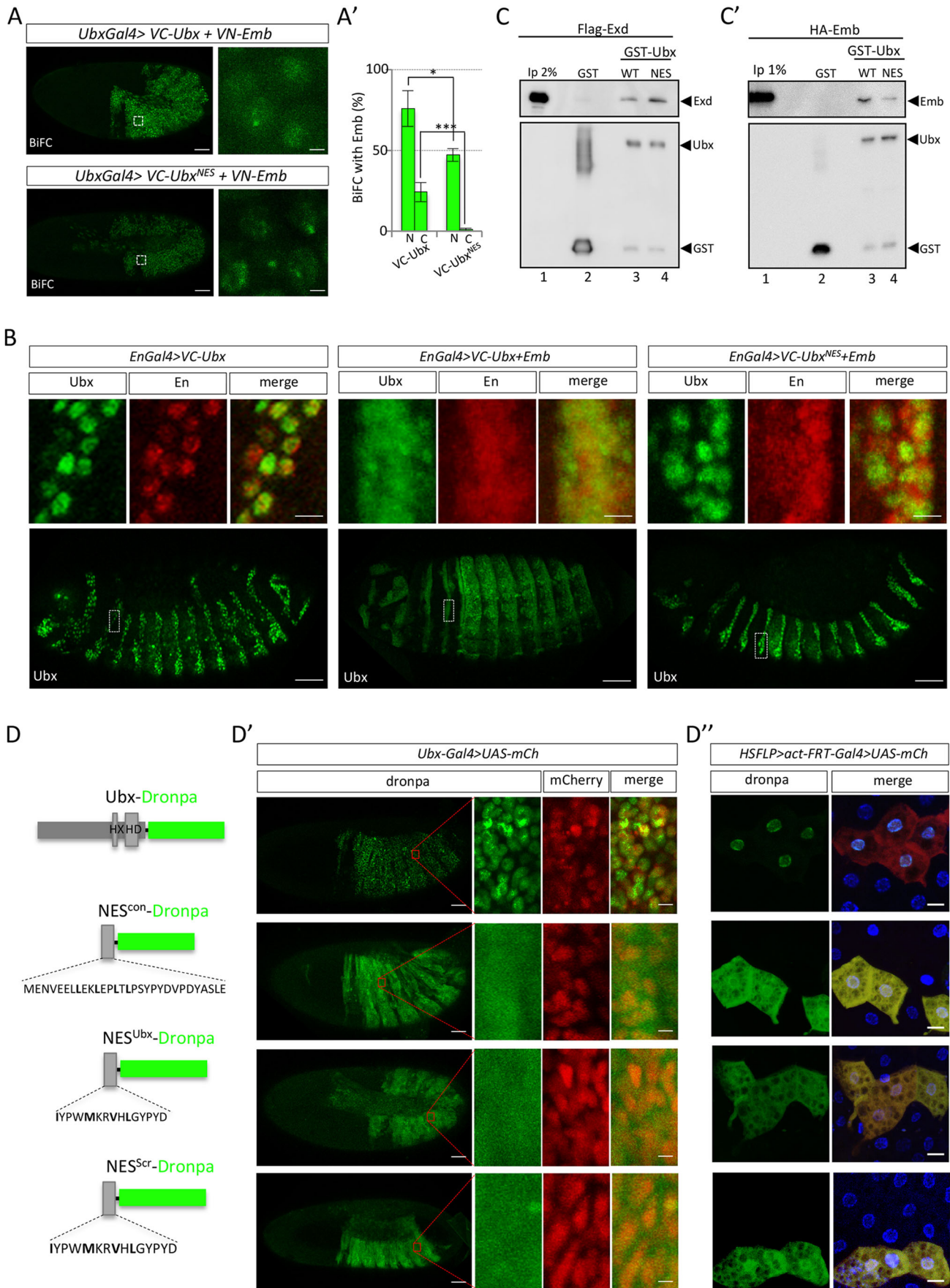
Fig. 3. See next page for legend.

Fig. 3. The unconventional NES of Ubx mediates its interaction with the *Drosophila* exportin Emb. (A,A′) Bimolecular fluorescence complementation (BiFC) between wild-type or NES-mutated Ubx and Embargoed (Emb). Fusion proteins are fused to the N- (VN) or C- (VC) terminal fragment of Venus and expressed with *Ubx-Gal4*, as indicated. BiFC was quantified (percentage relative signal) in the nucleus (N) and cytoplasm (C) of stage 10 live embryos (graph in A′) as is presented as mean±s.d. (*n*=23). The NES mutation abolishes BiFC is in the cytoplasm where ∼40% of fluorescence is lost in the nucleus. The difference in BiFC between conditions was evaluated (*$P<0.05$, ***$P<0.001$; *t*-test). Scale bars: 60 µm (full embryo); 3 µm (enlargement). See also Fig. S4 for nuclear and cytoplasmic BiFC quantification in live embryos. (B) Forced co-expression of Emb induces NES-dependent cytoplasmic localization of Ubx. The VC–Ubx fusion proteins (green) were expressed in the anterior part of parasegments of the embryo with the *engrailed* (*en*)-*Gal4* driver, with or without non-fluorescent HA-tagged Emb, as indicated. Immunostaining of VC–Ubx was performed with an anti-Ubx antibody in the T3 segment. The effect of Emb is also visible with anti-En staining (red), which becomes cytoplasmic in the presence of Emb. Mutation of the NES renders Ubx insensitive to the effect of Emb. This effect was significant ($P<0.001$; *t*-test). Scale bars: 40 µm (full embryo); 5 µm (enlargement). (C,C′) Immunoblots of GST pulldown assay using *in vitro* produced GST-fused derivatives (GST alone; GST-Ubx-wild type, WT; GST–Ubx-NES-mutated, NES) and whole S2R+ cell extracts expressing Flag–Exd (C) or HA–Emb (C′). Anti-HA antibody was used to recognize HA–Emb. Anti-Flag antibody was used to recognize Flag–Exd. Inputs (Ip) are systematically loaded, as indicated (first lane of each gel). Pulldown assays showed that Ubx-WT and Ubx-NES could interact with Exd and Emb (lanes 3,4). Quantification of interactions relative to GST–Ubx signal indicates that the interaction between Emb and Ubx–dNES is decreased by 55% on average when compared to the Ubx-WT form. In contrast, the NES mutation did not affect the interaction with Exd. The quantification was undertaken from three independent experiments and significance calculated with a one-way ANOVA test. (D–D″) W-containing motif peptides from Ubx and Scr behave as autonomous NESs when fused to the fluorescent Dronpa protein. (D) Schematic representation of the different constructs, with the peptide sequence fused to Dronpa in each case. Fusion with a consensus NES or full-length Ubx was used as a control. (D′) Expression of the fluorescent Dronpa fusion proteins in live *Drosophila* embryos. An illustrative confocal capture is provided in each case. Enlargements are shown on the right. Fusions are expressed with the *Ubx-Gal4* driver, together with NLS-mCherry to label the nuclei. The Ubx–Dronpa fusion protein is expressed in the nucleus, as expected. In contrast, the fusion to a consensus NES leads to the cytoplasmic localization of Dronpa. Peptides containing the non-canonical NES from Ubx and Scr also induce cytoplasmic localization of Dronpa, as efficiently as the consensus NES peptide. These effects were systematically observed in all embryos. Scale bars: 60 µm (full embryo); 10 µm (enlargement). (D″) Expression of fluorescent Dronpa fusion proteins in the fat body of L3-F stage larva. Clones expressing the fusion were induced from L1 to L3 larval stages through leaky expression from the HSFLP promoter and are recognized with the mCherry reporter (red) and Dronpa signal (green). Nuclei are stained with DAPI (blue). Consensus NES and HX-containing peptides trigger the Dronpa fluorescent protein to localize in the cytoplasm, as observed in the embryo. These effects were systematically observed in all fat bodies. Scale bars: 15 µm.

means of RNAi at the L3-W stage, using the same clonal expression system as previously described (Banreti et al., 2014). In this genetic background, we observed a nuclear retention of endogenous Ubx, exclusively in the *emb*-depleted cells, confirming that Emb was responsible for the Ubx nuclear export at the L3-W stage (Fig. 4A). We also observed retention of the mCherry–Atg8 reporter in the nucleus, with the absence of cytoplasmic autophagosomes, suggesting that the mCherry–Atg8 reporter was not fully repressed but could not be properly exported in the absence of Emb (Fig. 4A). To further validate that retention of endogenous Ubx in the nucleus of L3-W fat body cells was not due to a developmental delay induced by the absence of Emb, we co-expressed the VC–Ubx^{dN235dC} construct in *emb*-depleted cells. In this context, the VC–Ubx^{dN235dC} construct was retained in the nucleus of *emb*-depleted cells and able to repress autophagy

(Fig. 4A). This result showed that active export and degradation of the Ubx deleted form was dependent on Emb at the W stage.

To verify that active nuclear export was tightly linked to active degradation at L3-W stage, we inhibited the protein degradation machinery by clonally expressing a RNAi against the Cullin (Cul) ubiquitin ligase encoding gene at the L3-W stage. In *cul*-depleted cells, we observed endogenous Ubx and a significant repression of autophagy (Fig. 4B). This result reveals that Ubx nuclear export leads to the cytoplasmic degradation of the protein. Stabilizing Ubx in the cytoplasm could allow the protein to return into the nucleus, therefore inducing the repression of *atg* gene expression, which would eventually affect the formation of autophagosomes.

Altogether, our observations highlight that active Emb-dependent nuclear export is occurring in the transition from L3-F to L3-W fat body tissue to exclude Hox proteins from the nucleus and release the transcriptional repression of *atg* genes.

The N-terminal part of Ubx contains long intrinsically disordered regions (IDRs), which are inherent molecular features of Hox proteins (Merabet and Dard, 2014). These regions are more generally described to be under alternative splicing and post-translational modifications, allowing SLiMs to engage context-specific interactions with surrounding partners (Davey et al., 2012). Here, an important role of the disordered region resides is its ability to mask the NES, keeping Ubx active for repressing autophagy at the L3-F stage. This observation underlines that IDRs could positively influence the interaction potential of a regulatory protein by regulating its subcellular location and in particular in the case of Ubx by inhibiting the recruitment of Emb. Several post-translational modifications have been described to either promote or inhibit the activity of NES in TFs. Among them are the phosphorylation (Poon and Jans, 2005), sumoylation (Ptak and Wozniak, 2017), O-GlcNac modification (Özcan et al., 2010) and acetylation (Dai et al., 2015; Wang et al., 2010). These post-translational modifications could potentially be involved in the NES masking activity of the N-terminal region. Along this line, Ubx is phosphorylated throughout embryogenesis (Gavis and Hogness, 1991) and HOX proteins are described to interact with the CBP and p300 (CBP/p300) acetyl transferase proteins (Shen et al., 2001). Such post-translational modifications could potentially be involved in the NES-masking activity of the Ubx N-terminal region and we therefore performed a pilot screen by clonally expressing RNAi constructs targeting genes encoding for different kinases and CBP/p300 (herein referring to the fly protein Nejire) at the L3-F stage (see Materials and Methods and Fig. S5). The rational was that the inhibition of post-translational modifications involved in the NES-masking activity could lead to an nuclear export of Hox proteins, thereby inducing autophagy at the L3-F stage. We observed that Ubx staining was affected in the nucleus, but also visible in the cytoplasm of *CBP/p300-RNAi*-expressing cells at the L3-F stage (Fig. 4C). Analysis of mCherry–Atg8 revealed the formation of autophagy vesicles in the same *CBP/p300-RNAi* expressing cells (Fig. 4C), suggesting that anticipated autophagy could result from anticipated Hox nuclear export. Cytoplasmic localization was further confirmed by co-expressing the VC–Ubx construct in *CBP/p300*-depleted cells, highlighting that the degradation machinery was not effective at the L3-F stage (Fig. 4C). In this context, the VC–Ubx construct was not able to repress autophagy since small vesicles were also observed (Fig. 4C). In contrast, the NES-mutated form of Ubx was properly expressed in the nucleus of *CBP/p300*-depleted cells and the mCherry–Atg8 reporter was also fully repressed (Fig. 4C). Together, these results show that acetylation by CBP/p300 could constitute a protein mark participating in the mask of the NES during the L3-F stage.
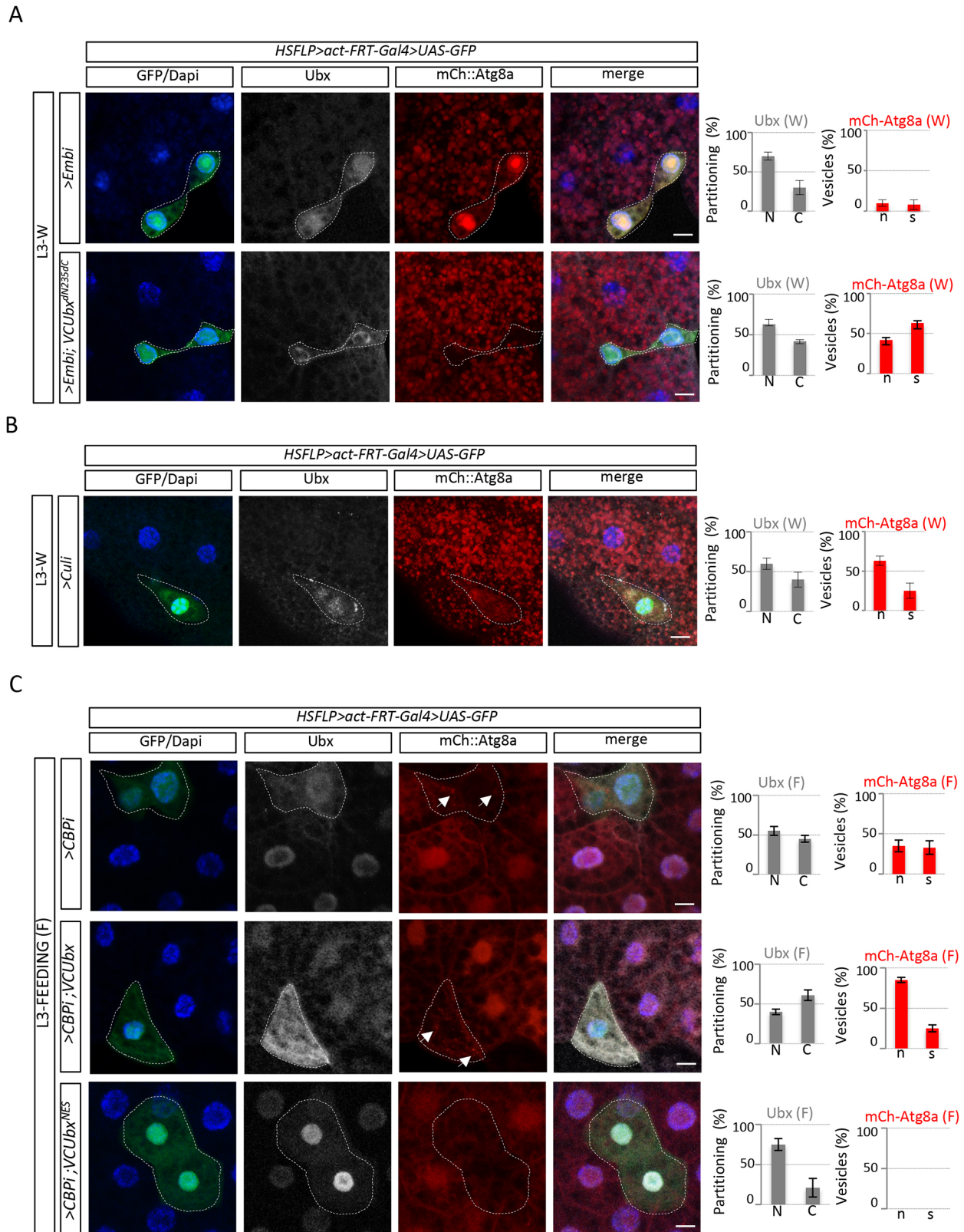
Fig. 4. See next page for legend.

DISCUSSION

Hox proteins are major regulators of developmental autophagy, acting as transcriptional repressors of *atg* genes (Banreti et al., 2014). The absence of Hox proteins in fat body nuclei of L3-W larvae coincides with the transcriptional activation of *atg* genes and the onset of autophagy. Therefore, Hox genes have to be transcriptionally repressed (Banreti et al., 2014), but Hox proteins present in the nucleus have also to be actively removed for releasing the repression of *atg* genes and allowing the induction of autophagy at the L3-W stage. Our work showed that the W-containing motif is

Fig. 4. Ubx is actively exported from fat body nuclei and degraded in the L3-W stage. (A) Blocking the nuclear export by inhibiting the expression of *Emb* with RNAi (*Embi*) leads to nuclear accumulation of endogenous Ubx in the nucleus of L3-W fat body cells. Note that mCherry–Atg8 reporter (mCh:: Atg8a) also accumulates in the nucleus. Co-expression of the VC–Ubx^{dN235dC} construct with the RNAi of Emb blocks nuclear export and degradation, allowing the construct to repress autophagy. Graphs on the right show the quantification of Ubx and mCherry–Atg8 distribution as described in the Fig. 1. (B) Blocking the proteasome activity through the expression of *Cullin* RNAi (*Culi*) reveals accumulation of endogenous Ubx and significant repression of autophagy in L3-W fat body cells. Graphs on the right show the quantification of Ubx and mCherry–Atg8 distribution as described in the Fig. 1. (C) Blocking acetylation by inhibiting the expression of *CBP/p300* with RNAi (*CBPi*) induces anticipated nuclear export of endogenous Ubx and autophagy at the L3-F stage. Loss of CBP induces a strong cytoplasmic localization of co-expressed wild-type VC–Ubx, with anticipated autophagy. In contrast, the co-expression of the NES-mutated form of VC-Ubx with CBPi did not lead to cytoplasmic localization, showing that Ubx nuclear export induced by the loss of CBP is fully dependent on the unconventional NES. Arrows highlight mCherry–Atg8 autophagy vesicles. Graphs on the right show the quantification of Ubx and mCherry–Atg8 distribution as described in Fig. 1. Clones with expression of fusion protein and RNAi are outlined with dashed lines and were induced as in Fig. 1. Scale bars: 10 μm.

part of an unconventional NES that is responsible for the nuclear export of the Hox protein Ubx at the L3-W stage. This activity relies on the Emb exportin protein and is masked during the L3-F stage (Fig. 5A). The acetyl transferase CBP/p300 participates in the masking mechanism, suggesting that acetylation/deacetylation is a way to control Ubx nuclear export in the larval fat body cells. Whether the same regulatory mechanism also applies to other Hox proteins remains to be resolved. The observation that autophagy was advanced upon the simple loss of *CBP/p300* suggests that acetylation could regulate the nuclear export of other Hox proteins. In addition, the induction of autophagy despite the constitutive expression of VC–Ubx in *CBP/p300*-depleted cells (in both the nucleus and cytoplasm) suggests that CBP/p300 could also act by modifying the transcriptional activity of Ubx.

Finally, the finding that the W-containing motif is part of a NES was surprising since this motif works as a critical docking platform for the PBC class cofactors in the context of Hox–PBC dimeric complexes (Fig. 5B). This role is however dispensable in the presence of the third partner Meis, which is required for the nuclear translocation of PBC proteins (Merabet and Mann, 2016). The dispensability of the W-containing motif in the context of the Hox–PBC–Meis trimeric complexes has been observed for the majority of Hox proteins studied so far (Dard et al., 2018), suggesting that the W-containing motif could be available for other types of interactions. Accordingly, the W-containing motif has been described to promote or reversely inhibit the interaction with different types of TFs (Fig. 5B), and this dual activity is tissue specific (Baëza et al., 2015). The role of the W-containing motif as part of a docking platform for the Emb/CRM1 exportin protein enlarges the repertoire of its putative binding partners (Fig. 5B). This role was described for Ubx and Dfd, but no NES-like signature could be identified in the W-containing region of AbdA or AbdB, which are also autophagy repressors during the L3-F stage (Banreti et al., 2014). This suggests that the control of Hox nuclear export in the fat body could rely on NESs that are not systematically located in the W-containing region, highlighting that the control of a generic Hox function could rely on different peptide motifs. It is interesting to note that mutating the NES in Ubx, Dfd and Scr mostly abolished the interaction with Emb/CRM1 in the cytoplasm, suggesting that other motif(s) could be required for the interaction in the nucleus. CRM1 has recently been described to promote the recruitment of the Nup98–HOXA9 fusion protein on

chromatin, and more specifically on Hox cluster regions in mouse embryonic stem cells (Oka et al., 2016). This observation underlines that CRM1 could also act as a Hox cofactor on DNA. In this context, Hox proteins could potentially use different CRM1-binding motif(s) to distinguish between the two activities (nuclear export or gene regulation) with the same cofactor.

In conclusion, our work, together with previous work, highlights the astonishing level of context-dependent protein interaction flexibility for the W-containing motif (Fig. 5B). These inherent molecular properties may explain why this short motif is conserved in the large majority of Hox proteins in animals, underlining that sequence conservation is not only compatible but also indispensable for functional diversity. Such molecular diversity implies a tight control by the other surrounding protein regions, including the non-conserved IDRs. The role of IDRs can explain why the same short peptide motif can have distinct and various functions in different protein contexts (Merabet and Hudry, 2011).

MATERIALS AND METHODS
Fly stocks
The different *Gal4* drivers used are: *Ubx-Gal4^{M1}* (de Navas et al., 2006), *engrailed(en)-Gal4* (Orihara et al., 1999), *Antp-Gal4* (Hudry et al., 2012). *UAS-RNAi* constructs were from Vienna [*UAS-EmbRNAi, P(KK102552)*] or Bloomington [*UAS-Cul1RNAi, P(Trip.HM05197); UAS-NemoRNAi, P(KK104885); UAS-PKA-C3RNAi, P(Trip.JF02723); UAS-NemoRNAi, P(KK104885); UAS-CKIIRNAi,P(KK106845); UAS-CBPRNAi, P(KK105115)*] stock centers.

The UAS-driven fly lines *UAS-VC-Ubx UAS-VC-Scr*, *UAS-VC-Scr^W* were previously generated (Hudry et al., 2012). The following UAS-driven fly lines were generated in this study: NES- and/or deleted forms of *UAS-VC-Ubx*, *UAS-HA/VC/VN-Emb*, *UAS-VN-Dfd/Dfd^W* and *UAS-Dronpa* constructs. All constructs were sequence-verified before transgenesis.

Flip-out expression of UAS constructs and mitotic clones and quantitation of protein localization and autophagy
Clonal expression and quantifications in fat body cells were performed as previously described (Banreti et al., 2014). Briefly, males carrying UAS constructs were crossed to *yw,hs-Flp;r4-mCherry::Atg8a;Act>CD2>GAL4, UAS-GFPnls* females. Crosses were kept for 1 night for egg laying at room temperature. Thereafter, parents were removed and the tube was incubated at 25°C for 3 days. Leaky expression of the heat-shock inducible Flp led to random 'flip out' of the CD2 cassette, allowing Gal4 to be expressed and to activate the expression of UAS-driven transgenes and nuclear GFP (to identify the cellular clones). mCherry–Atg8a (mCh::Atg8a) was used for tracing autophagy activity in the whole fat body.

Quantification of protein localization in the nucleus and cytoplasm and autophagy were performed with FIJI. The size and the number of vesicles were measured on maximum projections. Steps were as follows. First, a mask was first created for clonal expressing cells (green channel), using a gaussian blur (sigma=1) and the appropriate threshold. The functions 'Close' and 'Fill holes' were used to fill the holes in the mask. Second, The surface of each clone was extracted with the '3D object counter' function, and the 'Image Calculator' with the 'AND' function was used to create an image containing only the vesicles present in the clones (green channel mask AND max projection of the vesicles in the red channel). Third, an appropriate threshold was applied and the 'Watershed' function applied to separate vesicles. The surface and number of vesicles was extracted by using the '3D object counter' function, as previously. Finally, the same type of measurement was applied in surrounding wild-type (GFP-negative) cells: a mask was created for the zone containing the vesicles and the 'Fill' function was applied. The 'Image calculator' and 'Subtract' function were used to remove the GFP-positive clones from this mask, allowing measuring the surface outside the clonal expressing cells. This mask was combined with the red channel to create an image containing only vesicles outside the clones (using the 'AND' function). The surface and number of vesicles was extracted from this area with the '3D object counter' function.
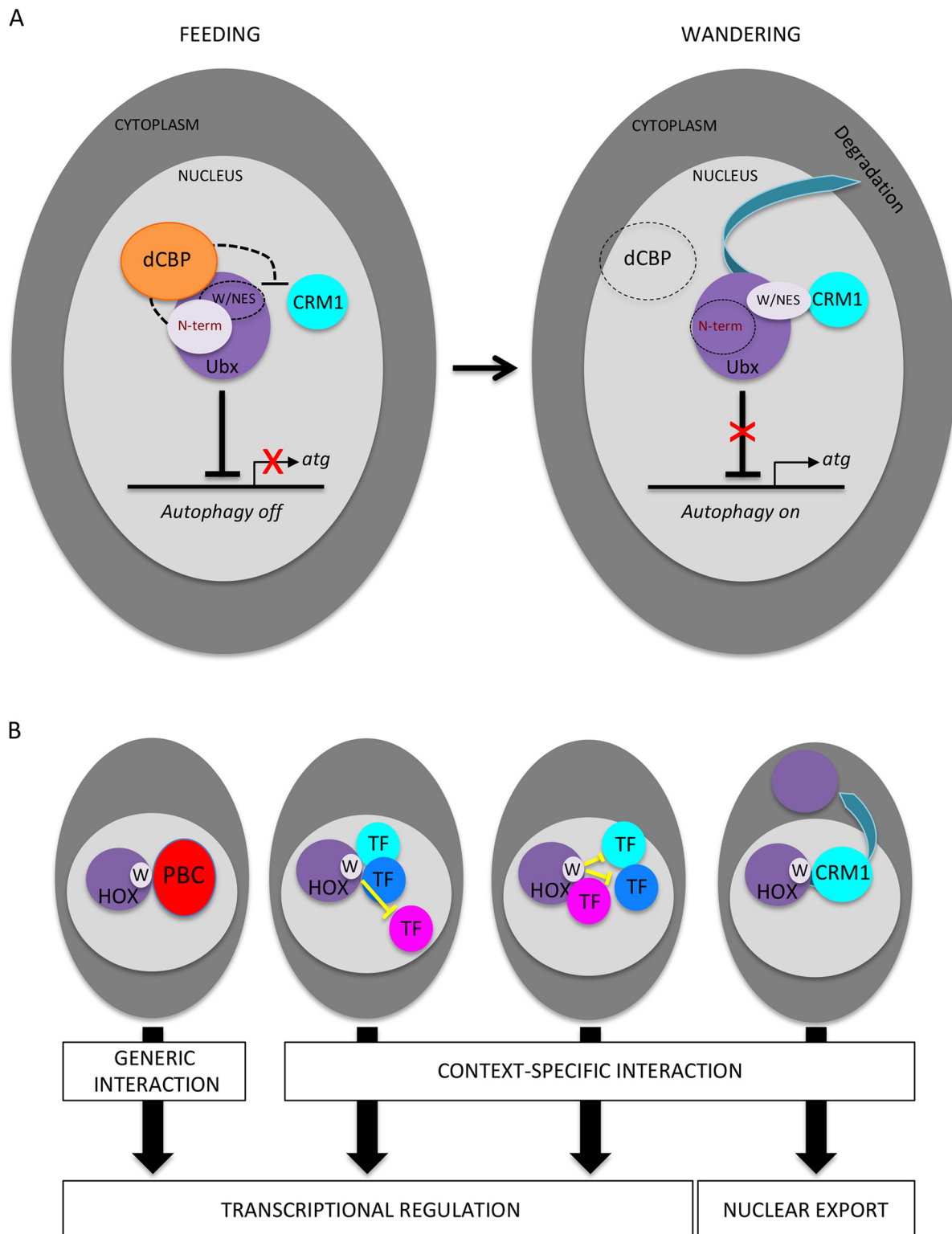
Fig. 5. The W-containing motif is involved in different types of molecular interactions to control context-dependent activity of Hox proteins. (A) The W-containing motif is part of an unconventional NES motif that controls the nuclear export of Ubx in the *Drosophila* larval fat body. Interaction between this NES and the Emb (CRM1) exportin protein is masked by the N-terminal part of Ubx at the L3-F stage. This masking mechanism depends on CBP/p300 (dCBP). The loss of CBP/p300 allows the interaction between the NES and Emb/CRM1, leading to the nuclear export and degradation of Ubx at the L3-W stage. Although it remains to be demonstrated, tight regulation of the nuclear export may generally apply to the other Hox proteins that repress autophagy. (B) The W-containing motif was originally described for its generic role in recruiting the PBC class cofactor in the context of Hox–PBC complexes (left panel). The W-containing motif was also shown to promote or inhibit interactions between Hox proteins and different transcription factors in the *Drosophila* embryo. This function is tissue specific, enabling the Hox protein to establish specific interaction networks in different environments (diagrams in middle panels; Baëza et al., 2015). Here, we present a novel tissue- and stage-specific (L3-W fat body) function of the W-containing motif, which participates in the Hox nuclear export through the interaction with the exportin CRM1/Emb (right panel).

At least three images from five animals and from three independent experiments were quantified for each genotype. The quantification number and size data were summarized in Excel and normalized to control levels (the average fluorescence, dot number and size of control cells were set to 100%).

Preparation of samples and imaging of fixed tissues
Larvae were dissected 4 days (L3 feeding stage) or 6 days (L3 wandering stage) after egg laying. Larval fat bodies were fixed at room temperature for 20 min in phosphate-buffered saline (PBS) containing 3.7% formaldehyde (formaldehyde methanol free, Thermo Fisher Scientific) and washed for 30 min in 1× PBS. All incubations were performed in PBS, with 2% BSA and 0.1% Triton X-100 at 4°C following standard procedures.

Images were acquired with a Zeiss LSM780 confocal microscope. Pictures were edited with ImageJ and Adobe Photoshop CS6 Version.

Cell culture and transfection
S2R+ *Drosophila* cells were thawed from the laboratory stock, tested for contamination and maintained at 25°C in Schneider medium supplemented with 10% FCS, 10 U/ml penicillin and 10 μg/ml streptomycin. Cells were simultaneously seeded and transfected with Effectene (Qiagen) according to the manufacturer's protocol. For the interaction assay, 10^7 cells were seeded in 100 mm dishes and transfected with *pActin-Gal4* and *UAS-nls-GFP*, *UAS-FLAG-Exd* or *UAS-HA-emb*. Cells were harvested in PBS after 48 h of transfection and pellets were resuspended with NP40 buffer (20 mM Tris-HCl pH 7.5, 150 mM NaCl, 2 mM EDTA and 1% NP40) supplemented with protease inhibitor cocktail (Sigma-Aldrich) and 1 mM of DTT and treated with benzonase (Sigma-Aldrich).

HEK293T cells were thawed from the laboratory stock, tested for contamination and transfected by using the JetPRIME reagent (Polyplus), with a total amount of 2 mg of DNA (1 mg of the HOXA5–mCherry and 1 mg of empty or CRM1–GFP-containing pcDNA3 vector). Coverslips were taken 20 h after transfection, at which time the fluorescence level is below saturation with each condition. Analysis was performed with a Zeiss LSM780 confocal microscope. Pictures correspond to the *Z*-projection of stacks, using the Zen software. Four to six different fields of cells were acquired under the same confocal parameters with the 20× objective from two independent experiments in each condition.

Constructs
All UAS constructs were sequence verified before fly transformation and transgenic fly lines were established with the ΦC31 integrase (Bischof et al., 2007). All UAS-Hox constructs were inserted on the same landing site on the second chromosome (22A3) as for the previous published UAS-Hox constructs (Hudry et al., 2012). UAS-Emb constructs were inserted on the third chromosome (62E1). HOXA5–mCherry, HOXA5^W–mCherry and CRM1–GFP were cloned in the pcDNA3 vector (Invitrogen) and are under the *CMV* promoter for expression.

Immunohistochemistry
Embryo collections and immunodetections were performed according to standard procedures.

The following primary antibodies used were: chicken anti-GFP (ab13970, Abcam, 1:500), rabbit anti-GFP (A11122, Molecular Probes, 1:500), mouse anti-Ubx (FP3.38, DSHB, 1:100) and rat anti-HA (11867423001, Roche, 1:500).

Secondary antibodies used for fluorescent revelation were conjugated to Alexa Fluor 488 (A11039; A11008, Molecular Probes), Cy-3 (A1051, Molecular probes), Alexa Fluor 647 (A21235, Invitrogen). Vectashield with DAPI (Vector Labs) was used to stain nuclear DNA.

SDS-PAGE and immunoblotting
For western blot analysis, proteins were resolved on 10% SDS-PAGE gels, blotted onto PVDF membrane (Bio-Rad) and probed with specific antibodies after saturation. The antibodies (and their dilution) used in this study were against: GST (2622, Cell Signaling Technology, 1:5000), Flag-M2 (F3165-.2MG Sigma-Aldrich, 1:1000), HA (3724, Cell Signaling Technology, 1:3000).

Protein purification and GST pulldown
Wild-type and mutated GST-tagged Ubx and Scr proteins were cloned in pGEX-6P plasmids (MERCK, #GE28-9546-48) and sequence verified before using. GST-tagged Ubx and Scr proteins were produced from the BL-21 (RIPL) bacterial strain, purified on gluthatione–Sepharose beads (GE Healthcare) and quantified by Coomassie staining. *In vitro* interaction assays were performed with equal amounts of GST or GST fusion proteins in affinity buffer (20 mM HEPES pH 7.9, 10 μM ZnCl$_2$, 0.1% Triton X-100 and 2 mM EDTA) supplemented with NaCl, 1 mM of DTT, 0.1 mM PMSF and protease inhibitor cocktail (Sigma-Aldrich). 300 μg of S2R+ whole cell lysates expressing nlsGFP, Flag–Exd or HA–Emb were subjected to interaction assays for 2 h at 4°C under mild rotation. Bound proteins were washed four times and resuspended in Laemmli buffer for western blot analysis. The input fraction was loaded as previously described (Carnesecchi et al., 2017).

GST pulldown experiments were quantified using FIJI software. Briefly, ratios of intensity of Exd or Emb proteins over GST bait signal were calculated and normalized to those for wild-type GST derivatives. Subsequent statistical analysis of Emb was performed with an one-way ANOVA test based on three biologically independent experiments (*n*=3).

BiFC visualization in live embryos
BiFC analysis was performed as previously described (Duffraisse et al., 2014). Briefly, embryos laid overnight were kept at 4°C for 24 h before live imaging. Living embryos were dechorionated and mounted in the halocarbon oil 10S (commercialized by VWR, Pennsylvania, USA). Images of BiFC in stage 10 live embryos were acquired with a Zeiss LSM780 confocal microscope, using filters adjusted for the Venus excitation (500 nm) and emission (535 nm) wavelengths. Identical parameters of acquisition were applied between the different genotypes. The number and intensity of the all pixels (for each embryo) were measured using the histogram function of the FIJI Software, as previously described (Duffraisse et al., 2014). Briefly, the threshold was adjusted appropriately with the 'Image calculator' function to create an image containing or excluding (using the 'Subtract' function) the nuclei. All selected areas were analyzed for fluorescence quantification ('Analyze particles' function) and number ('3D object counter' function). The intensity and number data were summarized in Excel and normalized to the values for wild-type (average dot intensity and number of control cells were set to 100%).

Supplementary information
Supplementary information available online at
https://jcs.biologists.org/lookup/doi/10.1242/jcs.241943.supplemental

Peer review history
The peer review history is available online at
https://jcs.biologists.org/lookup/doi/10.1242/jcs.241943.reviewer-comments.pdf

References

Adachi, Y. and Yanagida, M. (1989). Higher order chromosome structure is affected by cold-sensitive mutations in a Schizosaccharomyces pombe gene crm1+ which encodes a 115-kD protein preferentially localized in the nucleus and its periphery. *J. Cell Biol.* **108**, 1195-1207. doi:10.1083/jcb.108.4.1195

Baëza, M., Viala, S., Heim, M., Dard, A., Hudry, B., Duffraisse, M., Rogulja-Ortmann, A., Brun, C. and Merabet, S. (2015). Inhibitory activities of short linear motifs underlie Hox interactome specificity in vivo. *eLife* **4**, e06034. doi:10.7554/elife.06034

Banreti, A., Hudry, B., Sass, M., Saurin, A. J. and Graba, Y. (2014). Hox proteins mediate developmental and environmental control of autophagy. *Dev. Cell* **28**, 56-69. doi:10.1016/j.devcel.2013.11.024

Bischof, J., Maeda, R. K., Hediger, M., Karch, F. and Basler, K. (2007). An optimized transgenesis system for Drosophila using germ-line-specific phiC31 integrases. *Proc. Natl. Acad. Sci. USA* **104**, 3312-3317. doi:10.1073/pnas.0611511104

Carnesecchi, J., Forcet, C., Zhang, L., Tribollet, V., Barenton, B., Boudra, R., Cerutti, C., Billas, I. M. L., Sérandour, A. A., Carroll, J. S. et al. (2017). ERRα induces H3K9 demethylation by LSD1 to promote cell invasion. *Proc. Natl Acad. Sci. USA* **114**, 3909-3914. doi:10.1073/pnas.1614664114

Collier, S., Chan, H. Y. E., Toda, T., McKimmie, C., Johnson, G., Adler, P. N., O'Kane, C. and Ashburner, M. (2000). The Drosophila embargoed gene is required for larval progression and encodes the functional homolog of Schizosaccharomyces Crm1. *Genetics* **155**, 1799-1807.

Dai, J., Bercury, K. K., Jin, W. and Macklin, W. B. (2015). Olig1 acetylation and nuclear export mediate oligodendrocyte development. *J. Neurosci.* **35**, 15875-15893. doi:10.1523/JNEUROSCI.0882-15.2015

Dard, A., Reboulet, J., Jia, Y., Bleicher, F., Duffraisse, M., Vanaker, J. M., Forcet, C. and Merabet, S. (2018). Human HOX proteins use diverse and context-dependent motifs to interact with TALE class cofactors. *Cell Rep.* **22**, 3058-3071. doi:10.1016/j.celrep.2018.02.070

Davey, N. E., Van Roey, K., Weatheritt, R. J., Toedt, G., Uyar, B., Altenberg, B., Budd, A., Diella, F., Dinkel, H. and Gibson, T. J. (2012). Attributes of short linear motifs. *Mol. Biosyst.* **8**, 268-281. doi:10.1039/C1MB05231D

de Navas, L., Foronda, D., Suzanne, M. and Sánchez-Herrero, E. (2006). A simple and efficient method to identify replacements of P-lacZ by P-Gal4 lines allows obtaining Gal4 insertions in the bithorax complex of Drosophila. *Mech. Dev.* **123**, 860-867. doi:10.1016/j.mod.2006.07.010

Duffraisse, M., Hudry, B. and Merabet, S. (2014). Bimolecular fluorescence complementation (BiFC) in live Drosophila embryos. *Methods Mol. Biol.* **1196**, 307-318. doi:10.1007/978-1-4939-1242-1_19

Fornerod, M., Ohno, M., Yoshida, M. and Mattaj, I. W. (1997). CRM1 is an export receptor for leucine-rich nuclear export signals. *Cell* **90**, 1051-1060. doi:10.1016/S0092-8674(00)80371-2

Fukuda, M., Asano, S., Nakamura, T., Adachi, M., Yoshida, M., Yanagida, M. and Nishida, E. (1997). CRM1 is responsible for intracellular transport mediated by the nuclear export signal. *Nature* **390**, 308-311. doi:10.1038/36894

Fung, H. Y. J., Fu, S. C., Brautigam, C. A. and Chook, Y. M. (2015). Structural determinants of nuclear export signal orientation in binding to exportin CRM1. *eLife* **4**, e10034. doi:10.7554/eLife.10034

Fung, H. Y. J., Fu, S. C. and Chook, Y. M. (2017). Nuclear export receptor CRM1 recognizes diverse conformations in nuclear export signals. *eLife* **6**, e23961. doi:10.7554/eLife.23961

Galant, R., Walsh, C. M. and Carroll, S. B. (2002). Hox repression of a target gene: extradenticle-independent, additive action through multiple monomer binding sites. *Development* **129**, 3115-3126.

Gavis, E. R. and Hogness, D. S. (1991). Phosphorylation, expression and function of the Ultrabithorax protein family in Drosophila melanogaster. *Development* **112**, 1077-1093.

Hudry, B., Viala, S., Graba, Y. and Merabet, S. (2011). Visualization of protein interactions in living Drosophila embryos by the bimolecular fluorescence complementation assay. *BMC Biol.* **9**, 5. doi:10.1186/1741-7007-9-5

Hudry, B., Remacle, S., Delfini, M.-C., Rezsohazy, R., Graba, Y. and Merabet, S. (2012). Hox proteins display a common and ancestral ability to diversify their interaction mode with the PBC class cofactors. *PLoS Biol.* **10**, e1001351. doi:10.1371/journal.pbio.1001351

Kerppola, T. K. (2013). Bimolecular fluorescence complementation (BiFC) analysis of protein interactions in live cells. *Cold Spring Harb. Protoc.* **2013**, 727-731. doi:10.1101/pdb.prot076497

Lelli, K. M., Noro, B. and Mann, R. S. (2011). Variable motif utilization in homeotic selector (Hox)-cofactor complex formation controls specificity. *Proc. Natl. Acad. Sci. USA* **108**, 21122-21127. doi:10.1073/pnas.1114118109

Liu, Y., Matthews, K. S. and Bondos, S. E. (2008). Multiple intrinsically disordered sequences alter DNA binding by the homeodomain of the Drosophila hox protein ultrabithorax. *J. Biol. Chem.* **283**, 20874-20887. doi:10.1074/jbc.M800375200

Mann, R. S., Lelli, K. M. and Joshi, R. (2009). Chapter 3 Hox specificity: unique roles for cofactors and collaborators. *Curr. Top. Dev. Biol.* **88**, 63-101. doi:10.1016/S0070-2153(09)88003-4

Merabet, S. and Dard, A. (2014). Tracking context-specific transcription factors regulating hox activity. *Dev. Dyn.* **243**, 16-23. doi:10.1002/dvdy.24002

Merabet, S. and Hudry, B. (2011). On the border of the homeotic function: re-evaluating the controversial role of cofactor-recruiting motifs: the role of cofactor-recruiting motifs in conferring Hox evolutionary flexibility may critically depend on the protein environment. *Bioessays* **33**, 499-507. doi:10.1002/bies.201100019

Merabet, S. and Mann, R. S. (2016). To be specific or not: the critical relationship between Hox And TALE proteins. *Trends Genet.* **32**, 334-347. doi:10.1016/j.tig.2016.03.004

Merabet, S., Saadaoui, M., Sambrani, N., Hudry, B., Pradel, J., Affolter, M. and Graba, Y. (2007). A unique Extradenticle recruitment mode in the Drosophila Hox protein Ultrabithorax. *Proc. Natl. Acad. Sci. USA* **104**, 16946-16951. doi:10.1073/pnas.0705832104

Merabet, S., Hudry, B., Saadaoui, M. and Graba, Y. (2009). Classification of sequence signatures: a guide to Hox protein function. *Bioessays* **31**, 500-511. doi:10.1002/bies.200800229

Mooney, C., Pollastri, G., Shields, D. C. and Haslam, N. J. (2012). Prediction of short linear protein binding regions. *J. Mol. Biol.* **415**, 193-204. doi:10.1016/j.jmb.2011.10.025

Morgan, R., In der Rieden, P., Hooiveld, M. H. W. and Durston, A. J. (2000). Identifying HOX paralog groups by the PBX-binding region. *Trends Genet.* **16**, 66-67. doi:10.1016/S0168-9525(99)01881-8

Mukherjee, K. and Bürglin, T. R. (2007). Comprehensive analysis of animal TALE homeobox genes: new conserved motifs and cases of accelerated evolution. *J. Mol. Evol.* **65**, 137-153. doi:10.1007/s00239-006-0023-0

Oka, M., Mura, S., Yamada, K., Sangel, P., Hirata, S., Maehara, K., Kawakami, K., Tachibana, T., Ohkawa, Y., Kimura, H. et al. (2016). Chromatin-prebound Crm1 recruits Nup98-HoxA9 fusion to induce aberrant expression of Hox cluster genes. *eLife* **5**, e09540. doi:10.7554/eLife.09540

Orihara, M., Hosono, C., Kojima, T. and Saigo, K. (1999). Identification of engrailed promoter elements essential for interactions with a stripe enhancer in Drosophila embryos. *Genes Cells* **4**, 205-218. doi:10.1046/j.1365-2443.1999.00254.x

Özcan, S., Andrali, S. S. and Cantrell, J. E. L. (2010). Modulation of transcription factor function by O-GlcNAc modification. *Biochim. Biophys. Acta* **1799**, 353-364. doi:10.1016/j.bbagrm.2010.02.005

Poon, I. K. H. and Jans, D. A. (2005). Regulation of nuclear transport: central role in development and transformation? *Traffic* **6**, 173-186. doi:10.1111/j.1600-0854.2005.00268.x

Ptak, C. and Wozniak, R. W. (2017). SUMO and nucleocytoplasmic transport. *Adv. Exp. Med. Biol.* **963**, 111-126. doi:10.1007/978-3-319-50044-7_7

Rinaldi, L., Saurin, A. J. and Graba, Y. (2018). Fattening the perspective of hox protein specificity through slimming. *Int. J. Dev. Biol.* **62**, 755-766. doi:10.1387/ijdb.180306yg

Romero, N. M., Irisarri, M., Roth, P., Cauerhff, A., Samakovlis, C. and Wappner, P. (2008). Regulation of the Drosophila hypoxia-inducible factor α Sima by CRM1-dependent nuclear export. *Mol. Cell. Biol.* **28**, 3410-3423. doi:10.1128/MCB.01027-07

Roth, P., Xylourgidis, N., Sabri, N., Uv, A., Fornerod, M. and Samakovlis, C. (2003). The Drosophila nucleoporin DNup88 localizes DNup214 and CRM1 on the nuclear envelope and attenuates NES-mediated nuclear export. *J. Cell Biol.* **163**, 701-706. doi:10.1083/jcb.200304046

Saurin, A. J., Delfini, M. C., Maurel-Zaffran, C. and Graba, Y. (2018). The generic facet of Hox protein function. *Trends Genet.* **34**, 941-953. doi:10.1016/j.tig.2018.08.006

Shen, W.-F., Krishnan, K., Lawrence, H. J. and Largman, C. (2001). The HOX homeodomain proteins block CBP histone acetyltransferase activity. *Mol. Cell. Biol.* **21**, 7509-7522. doi:10.1128/MCB.21.21.7509-7522.2001

Stade, K., Ford, C. S., Guthrie, C. and Weis, K. (1997). Exportin 1 (Crm1p) is an essential nuclear export factor. *Cell* **90**, 1041-1050. doi:10.1016/S0092-8674(00)80370-0

Tour, E., Hittinger, C. T. and McGinnis, W. (2005). Evolutionarily conserved domains required for activation and repression functions of the Drosophila Hox protein Ultrabithorax. *Development* **132**, 5271-5281. doi:10.1242/dev.02138

Wang, H., Holloway, M. P., Ma, L., Cooper, Z. A., Riolo, M., Samkari, A., Elenitoba-Johnson, K. S. J., Chin, Y. E. and Altura, R. A. (2010). Acetylation directs survivin nuclear localization to repress STAT3 oncogenic activity. *J. Biol. Chem.* **285**, 36129-36137. doi:10.1074/jbc.M110.152777